Supplementary Information (SI) for Inorganic Chemistry Frontiers.

Supplementary materials

A purely inorganic germanium−molybdenum−oxo cluster with ruthenium participation for visible-light-driven CO_2 reduction

Kunhong Li, Yumei Hong, Xinyi Ma, Yujie Zhao, Shihao Zhang, Pengtao Ma, Jingyang Niu* and Jingping Wang*

Henan Key Laboratory of Polyoxometalate Chemistry, College of Chemistry and Molecular Sciences, Henan University, Kaifeng, Henan 475004, (P. R. China), E-mail: jyniu@henu.edu.cn, jpwang@henu.edu.cn

Table of contents

1 Supplementary Experimental Section.

1.1 Measurement of photocatalytic activity.

The photocatalytic reduction of CO_2 was conducted with a quartz glass reactor (CEL-APR100H-3, 100 mL) equipped with a Beijing China Education Au-light Technology Co., Ltd. 300 W xenon lamp (CEL-PF300-T6) with a UV-cutoff filter (≥ 420 nm) as the visible light source. In a typical experiment, 5 mg of the photocatalyst and 7.5 mg $[Ru(bpy)_3]Cl_2 \cdot 6H_2O$ were dispersed in 29 mL of the mixed solution of N,N-Dimethylformamide (DMF; 16 mL), H_2O (8 mL), and triethanolamine (TEOA; 5 mL), and pre-degassed with CO_2 (99.999%) gas for 30 min to remove air before irradiation. Here TEOA serves as a sacrificial agent and $[Ru(bpy)_3]Cl_2 \cdot 6H_2O$ acts as a photosensitizer. The reaction mixture was kept stirred constantly with a magnetic bar to ensure complete mixing of the photocatalyst particles. The temperature of the reaction was maintained at 20 °C by a cooling water. The gas product (0.5 mL, taken from the reactor) was analyzed using a gas chromatograph equipped with an FID and a TCD detector (Agilent GC-8890). The selectivity of the formed CO and CH_4 is calculated according to the following equation:

$$selectivity\ of\ CH_4 = \frac{8R(CH_4)}{8R(CH_4) + 2R(CO)} \times 100\%$$

$$selectivity\ of\ CO = \frac{2R(CO)}{8R(CH_4) + 2R(CO)} \times 100\%$$

where R(CO) and R(CH_4) are the yields of reactively-formed CO and CH_4 respectively.

1.2 The calculation of gas production (μmol·g^{-1}) and gas generation rate (μmol·g^{-1}·h^{-1}).

$$CH_4\ or\ CO\ production\ (\mu mol/g) = \frac{c(ppm) \times 10^{-6} \times V(mL) \times 10^{-3}}{22.4(L/mol) \times m(mg) \times 10^{-3}} \times 10^6 = \frac{c(ppm) \times V(mL)}{22.4(L/mol) \times m(mg)}$$

$$CH_4\ or\ CO\ yield\ rate\ (\mu mol/g/h) = \frac{c(ppm) \times 10^{-6} \times V(mL) \times 10^{-3}}{22.4(L/mol) \times m(mg) \times 10^{-3} \times t(h)} \times 10^6 = \frac{c(ppm) \times V(mL)}{22.4(L/mol) \times m(mg) \times t(h)}$$

c(ppm): the concentration of CH_4 or CO;

V(mL): the spare volume of photoreactor;

m(mg): the mass of photocatalyst;

t(h): the reaction time.

1.3 The calculation of apparent quantum yield (AQY).

The AQY is determined using a similar method to that for the photocatalytic performance test. Photocatalyst (5 mg), $[Ru(bpy)_3]Cl_2 \cdot 6H_2O$ (7.5 mg), N,N-Dimethylformamide (DMF; 16 mL), H_2O (8 mL), and triethanolamine (TEOA; 5 mL). The intensity of the incident light was tested by a photometer (CEL-NP2000-2A, Beijing China Education Au-light Technology Co., Ltd.), the irradiated area is 28.27 cm^2.

The apparent quantum efficiency yield (AQY) at 420 nm, 460 nm, 500 nm, and 550 nm is calculated on the basis of the following equation:

$$AQY\% = \frac{Number\ of\ reacted\ electrons\ (N_e)}{Number\ of\ incident\ photons\ (N_P)} \times 100\%$$

$$AQY\% = \frac{10^9 \times (\nu \times N_A \times K) \times (h \times c)}{(I \times A \times \lambda)} \times 100\%$$

$$= \frac{1.2 \times 10^8 (\nu \times K)}{(I \times A \times \lambda)} \times 100\%$$

According to the following chemical reactions:

$$CO_2 + 8e^- \rightarrow CH_4$$

$$CO_2 + 2e^- \rightarrow CO$$

the AQY for CH_4 and CO evolution under different wavelengths are evaluated by the following equation:

$$AQY(CH_4)\% = \frac{Number\ of\ CH_4\ molecules\ \times 8}{Number\ of\ incident\ photons} \times 100\%$$

$$AQY(CO)\% = \frac{Number\ of\ CO\ molecules\ \times 2}{Number\ of\ incident\ photons} \times 100\%$$

ν: the reaction rate ($mol \cdot s^{-1}$);

N_A: the Avogadro constant ($6.02 \times 10^{23}\ mol^{-1}$);

K: Number of Transferred electrons (CH_4 = 8; CO = 2);

h: the Planck constant ($6.626 \times 10^{-34}\ J \cdot s$);

c: the speed of light ($3 \times 10^8\ m \cdot s^{-1}$);

I: the incident light intensity at certain wavelength ($W \cdot m^{-2}$);

A: the irradiated area (m^2);

λ: the wavelength of incident light (nm);

1.4 Electrochemical measurements.

All the electrochemical studies were performed on an electrochemical workstation (CHI-760E, Shanghai, China) with a standard three-electrode system with a glassy carbon as the working electrode, a Pt plate as the counter electrode, and an Ag/AgCl electrode as the reference electrode. The as-synthesized samples (5 mg) were added into 470 μL ethanol and 30 μL Poly (diallyldimethylammonium chloride) mixed solution under sonication for 30 min. Subsequently, 30 μL of the mixed solution was covered onto the side of ITO glass, and dried in room temperature. Photocurrent-time (I-t) curve and electrochemical impedance spectra were measured in 0.5M Na_2SO_4 aqueous solution, where the I-t curve was performed under intermittent irradiation with a 300 W Xenon lamp source. High-purity N_2 was passed through the solution for at least 30 min to remove oxygen before the test.

1.5 photoluminescence (PL) measurements.

Photoluminescence (PL) spectra are scanned on a photoluminescence spectrometer (FLS980) under an excitation wavelength of 368 nm. The photoluminescent quenching of $[Ru(bpy)_3]Cl_2 \cdot 6H_2O$ (7.5 mg) were performed in 6 mL of the mixed solution of N,N-Dimethylformamide (DMF; 4 mL), H_2O (2 mL) upon the addition of increasing amounts of **$Ru_2Ge_2Mo_{20}$** (0.0 mg, 0.5 mg, 1.0 mg, 1.5 mg, and 2.0 mg). The photoluminescent quenching of $[Ru(bpy)_3]Cl_2 \cdot 6H_2O$ (7.5 mg) were performed in 6 mL of the mixed solution of N,N-Dimethylformamide (DMF; 4 mL), H_2O (2 mL) in different the amounts of TEOA (0 mM, 20 mM, 50 mM, and 100 mM).

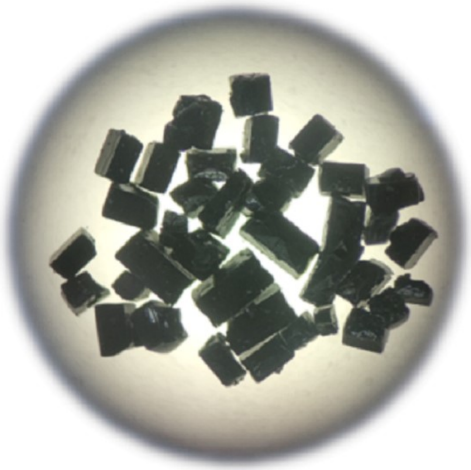

Fig. S1 The crystal image of **$Ru_2Ge_2Mo_{20}$** under an optical microscope.

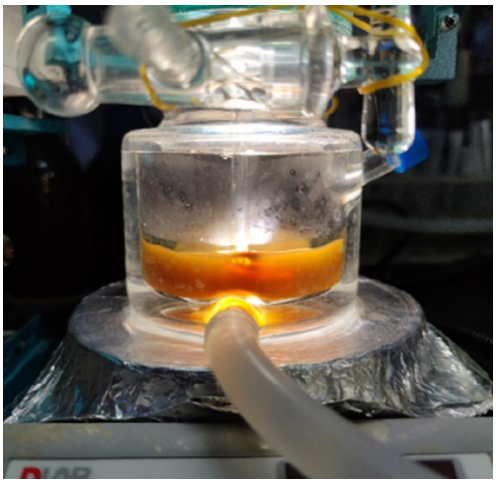

Fig. S2 The photograph of the CO_2 photoreduction quartz glass reactor.

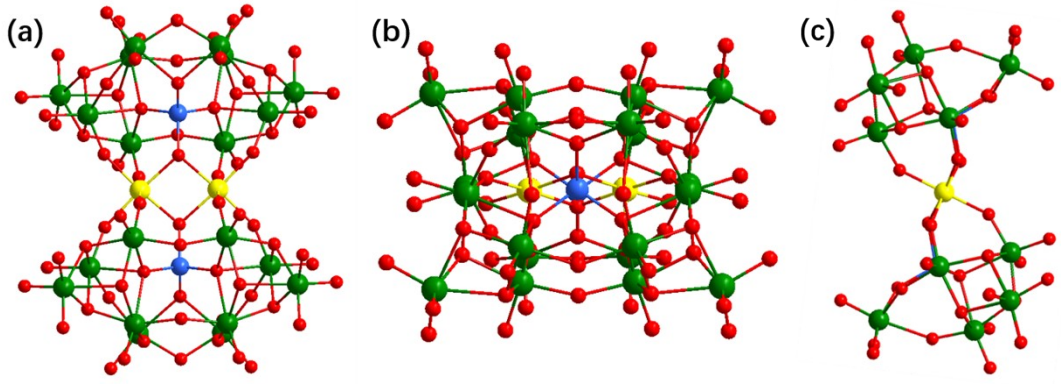

Fig. S3 (a) x-axis and (b) z-axis and (c) y-axis ball-and-stick representation of the **$Ru_2Ge_2Mo_{20}$**.

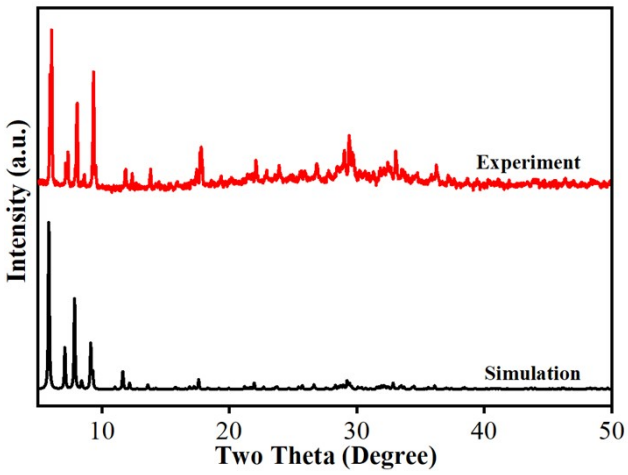

Fig. S4 Simulated and experimental PXRD patterns of **$Ru_2Ge_2Mo_{20}$**.

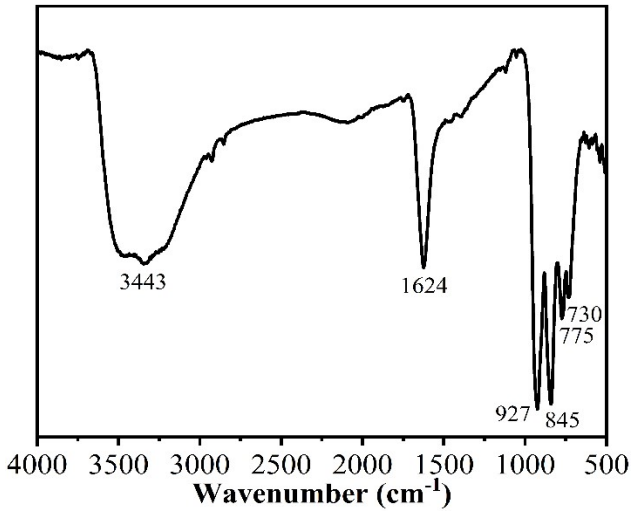

Fig. S5 IR spectrum of **$Ru_2Ge_2Mo_{20}$**.

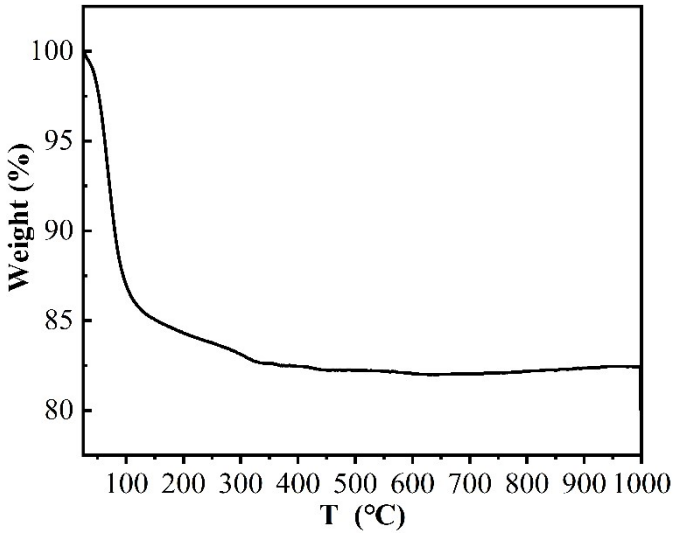

Fig. S6 TG curves of the **$Ru_2Ge_2Mo_{20}$**.

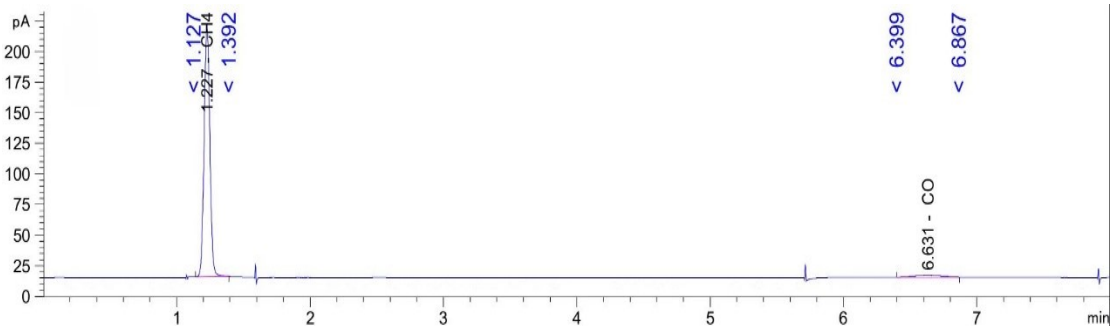

Fig. S7 GC profiles of CO_2 reduction after reaction 6 h under normal condition.
Chromatographic column information: HP-5 column, 30 m × 320 μm × 0.25 μm
Detection information: oven (80 °C), TCD (250 °C), FID (275 °C)

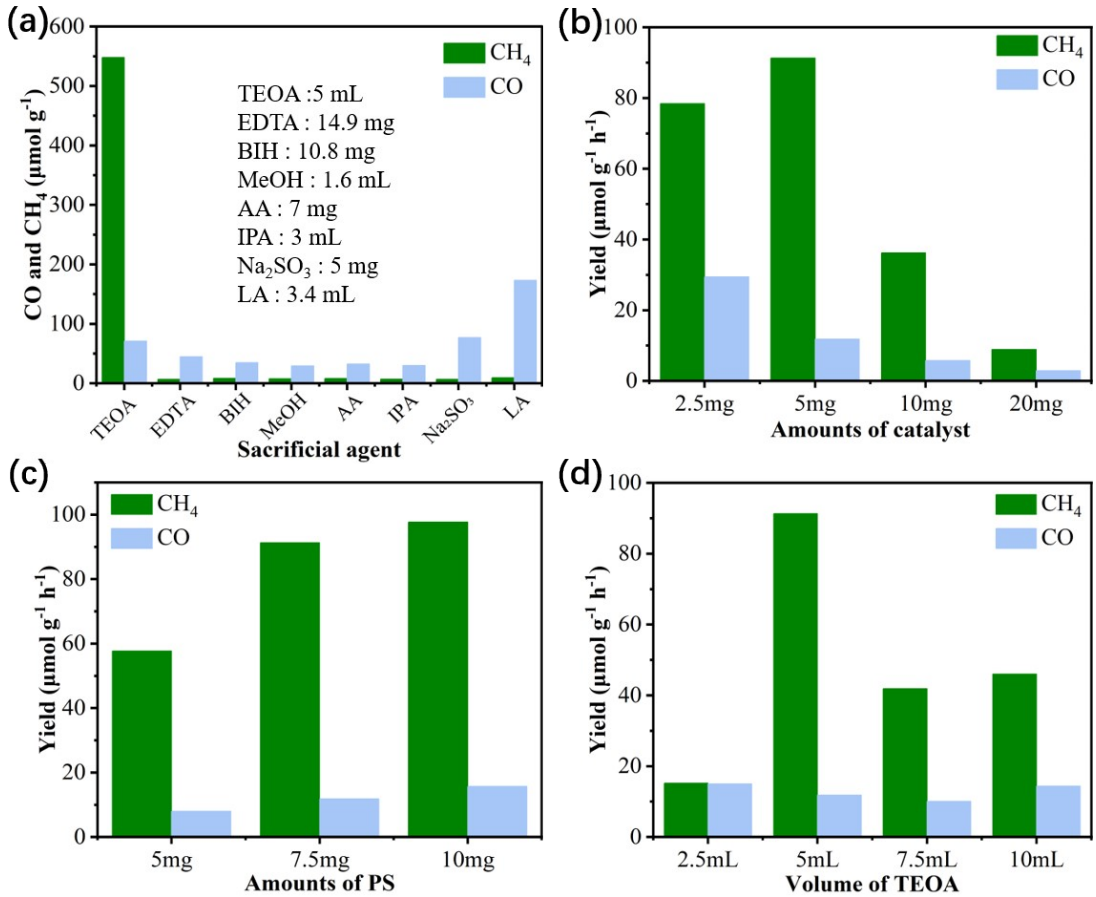

Fig. S8 CH_4 and CO production rates of photocatalytic CO_2 reduction with (a) different sacrificial donors, different amounts of (b) catalyst and (c) PS and (d) TEOA.

As shown in **Fig. S8c−d**, an excess of PS or TEOA would lead to an insignificant increase or decrease in the evolution rate of products.

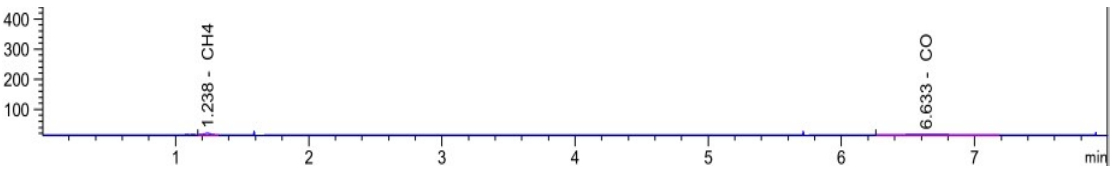

Fig. S9 GC profiles of CO_2 reduction after reaction 6 h under Ar condition.

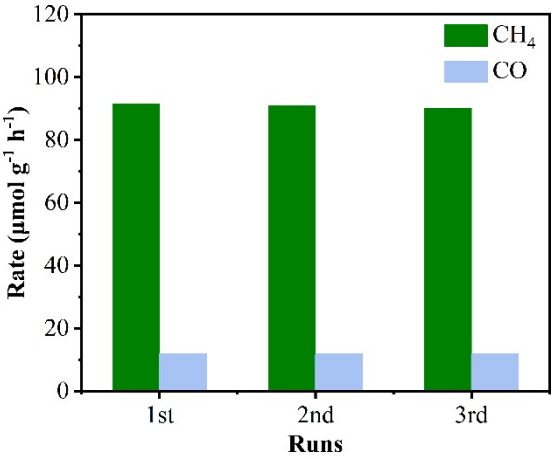

Fig. S10 Recyclability experiments.

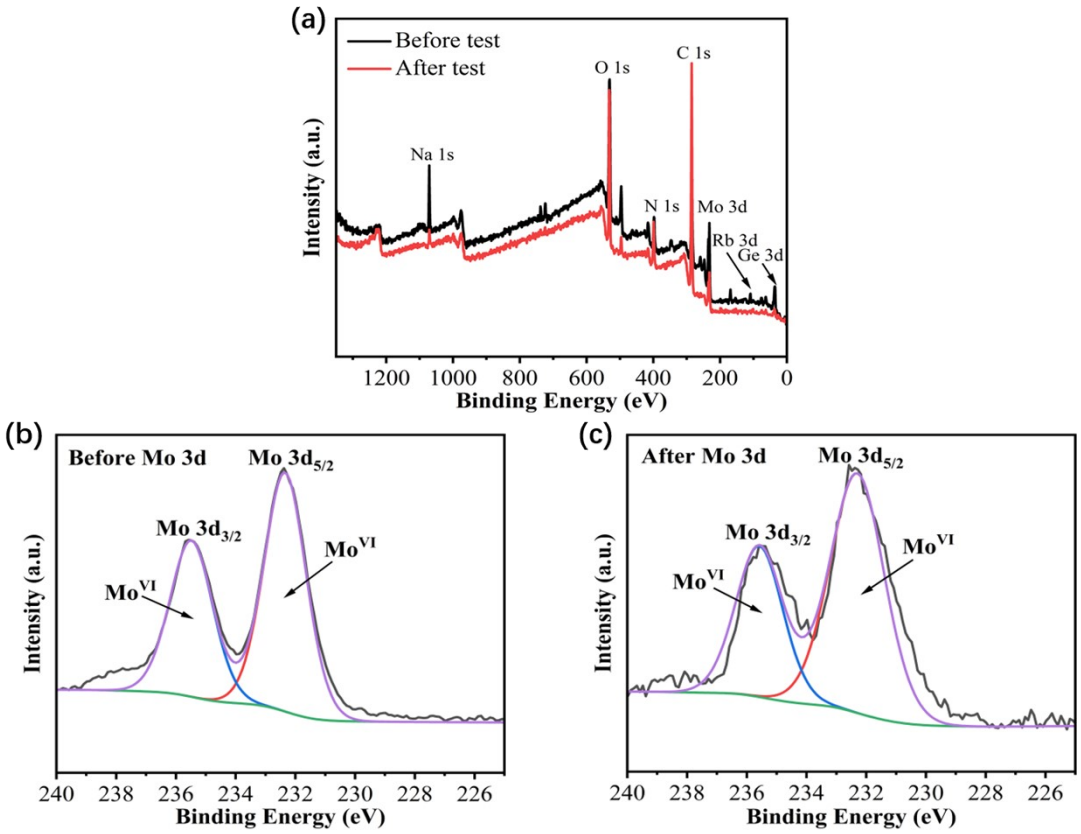

Fig. S11 (a) XPS spectra of the **$Ru_2Ge_2Mo_{20}$** before (black) and after (red) cycled reactions in survey scan. Mo3d XPS spectra (b) before and (c) after photocatalysis of the **$Ru_2Ge_2Mo_{20}$**.[1, 2]

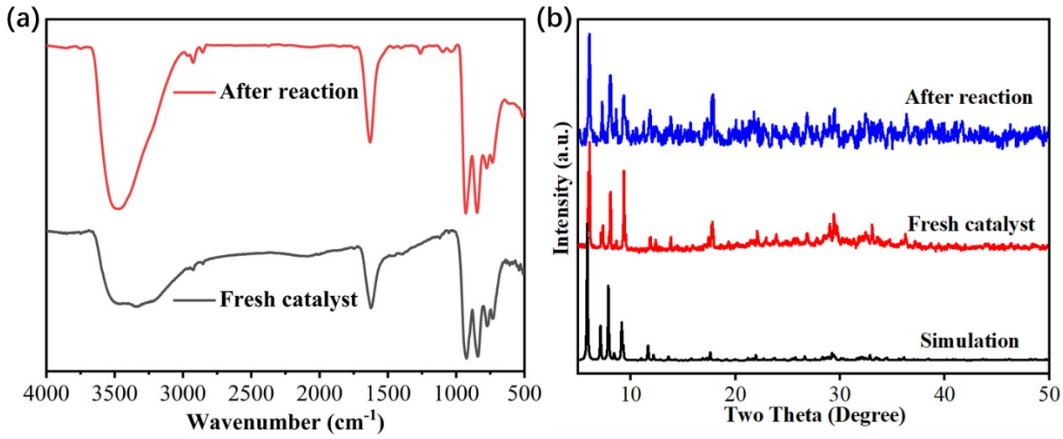

Fig. S12 (a) IR and (b) PXRD spectra of the **$Ru_2Ge_2Mo_{20}$** before and after the photocatalytic reaction.

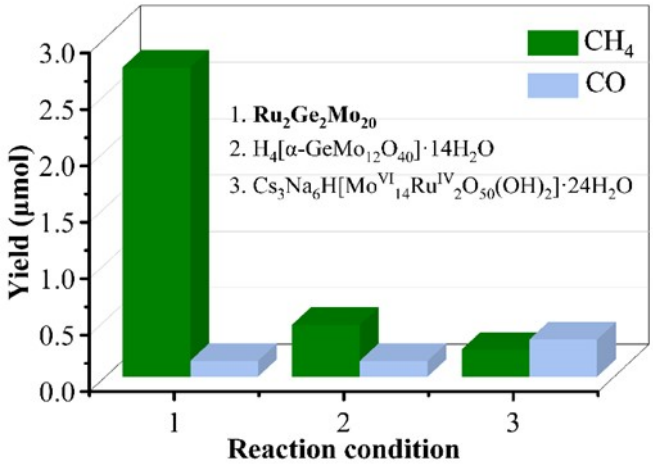

Fig. S13 Comparison results of different catalysts.

(Reaction condition: **1** or **2** or **3** (0.001 mmol), $[Ru(bpy)_3]Cl_2·6H_2O$ (7.5 mg), solution (DMF = 16 mL, H_2O = 8 mL, TEOA = 5 mL), CO_2 (0.1 MPa), ≥420 nm, 20 °C, 6 h.)

Table S1 Crystallographic data of the **$Ru_2Ge_2Mo_{20}$**.

Empirical formula	$Na_{12}Rb_2H_{88}Ge_2Ru_2Mo_{20}O_{120}$
Formula weight	4721.4132
Crystal system	orthorhombic
Space group	*P*nnm
a / Å	12.5569(4)
b /Å	19.0577(5)
c /Å	24.7605(8
$\alpha = \beta = \gamma$ /°	90
Volume / Å^3	5925.3(3)
Z	2
ρ_{calc} g / cm^3	2.597
μ / mm^{-1}	3.765

$F(000)$	4316.0
Crystal size / mm^3	0.16 × 0.08 × 0.06
Data/parameters	5403/18/369
R_{int}	0.0951
GOF on F^2	1.138
R_1, wR_2 [$I \geq 2\sigma(I)$]	0.0722, 0.1602
R_1, wR_2 [all data]	0.0866, 0.1677

Table S2 Major bond lengths (Å) and bond angles (°) of the **$Ru_2Ge_2Mo_{20}$**.

Bond	Length	Bond	Length	Bond	Length
Ge1–O1	1.761(12)	Mo2–O11	1.757(9)	Mo5–O2	1.788(8)
Ge1–O6	1.757(9)	Mo2–O16	1.688(9)	Mo5–O3	1.898(4)
Ge1–O6	1.757(9)	Mo3–O11	2.291(9)	Mo5–O4	2.002(8)
Ge1–O13	1.764(13)	Mo3–O12	1.915(10)	Mo5–O6	2.295(8)
Mo1–O5	1.788(8)	Mo3–O13	2.225(8)	Mo5–O8	2.071(9)
Mo1–O6	2.282(9)	Mo3–O14	1.935(7)	Mo5–O10	1.717(9)
Mo1–O7	2.052(9)	Mo3–O20	1.733(11)	Mo5–Rb1	4.105(2)
Mo1–O8	2.025(9)	Mo3–O21	1.726(9)	Mo5–Rb1	4.208(3)
Mo1–O12	1.897(10)	Mo4–O4	2.266(9)	O1–Ru1	2.059(8)
Mo1–O15	1.726(10)	Mo4–O7	2.219(10)	O2–Ru1	2.003(8)
Mo2–O4	2.085(9)	Mo4–O8	2.181(9)	O5–Ru1	1.996(8)
Mo2–O6	2.305(8)	Mo4–O17	1.745(10)	Mo2–O9	1.897(4)
Mo2–O7	2.030(10)	Mo4–O18	1.746(10)	Mo4–O19	1.748(10)
Bond	Angle	Bond	Angle	Bond	Angle
O1–Ge1–O13	109.5(6)	O16–Mo2–O6	170.7(4)	O18–Mo4–O19	104.6(5)
O6–Ge1–O1	108.1(3)	O16–Mo2–O7	100.5(5)	O19–Mo4–O4	90.0(4)
O5–Mo1–O6	84.3(3)	O16–Mo2–O9	99.2(5)	O19–Mo4–O7	91.3(4)
O5–Mo1–O8	90.5(4)	O16–Mo2–O11	103.9(5)	O19–Mo4–O8	154.8(4)
O5–Mo1–O12	99.0(4)	O12–Mo3–O11	79.7(4)	O2–Mo5–O3	97.1(4)
O7–Mo1–O6	75.2(3)	O12–Mo3–O13	83.9(4)	O2–Mo5–O4	155.1(4)
O8–Mo1–O6	75.5(3)	O12–Mo3–O14	152.3(5)	O2–Mo5–O6	82.9(3)
O8–Mo1–O7	75.7(4)	O13–Mo3–O11	79.1(4)	O2–Mo5–O8	88.6(4)
O12–Mo1–O6	81.9(4)	O14–Mo3–O11	81.4(5)	O3–Mo5–O4	90.9(4)
O12–Mo1–O7	87.3(4)	O14–Mo3–O13	72.8(4)	O3–Mo5–O6	85.8(4)
O12–Mo1–O8	154.5(4)	O20–Mo3–O11	85.5(4)	O3–Mo5–O8	158.6(4)
O15–Mo1–O5	102.2(4)	O20–Mo3–O12	101.4(5)	O4–Mo5–O6	74.1(3)
O15–Mo1–O6	172.5(4)	O20–Mo3–O13	162.6(5)	O4–Mo5–O8	76.1(4)
O15–Mo1–O7	97.7(4)	O20–Mo3–O14	97.1(5)	O8–Mo5–O6	74.4(3)
O15–Mo1–O8	100.6(4)	O21–Mo3–O11	170.9(4)	O10–Mo5–O2	102.7(4)
O15–Mo1–O12	100.4(5)	O21–Mo3–O12	96.7(5)	O10–Mo5–O3	99.5(5)

O4–Mo2–O6	72.4(3)	O21–Mo3–O13	92.3(5)	O10–Mo5–O4	99.2(4)
O7–Mo2–O4	77.3(4)	O21–Mo3–O14	98.9(6)	O10–Mo5–O6	171.6(4)
O7–Mo2–O6	75.1(3)	O21–Mo3–O20	103.4(5)	O10–Mo5–O8	99.3(4)
O9–Mo2–O4	87.6(4)	O7–Mo4–O4	70.0(3)	Ge1–O1–Ru1	122.3(4)
O9–Mo2–O6	83.6(4)	O8–Mo4–O4	68.7(3)	Ru1–O1–Ru1	95.0(5)
O9–Mo2–O7	156.7(4)	O8–Mo4–O7	69.3(3)	Mo5–O2–Ru1	145.6(5)
O11–Mo2–O4	155.8(4)	O17–Mo4–O4	155.3(4)	Mo5–O3–Mo5	146.9(7)
O11–Mo2–O6	84.5(4)	O17–Mo4–O7	88.5(4)	Mo2–O4–Mo4	100.0(4)
O11–Mo2–O7	90.1(4)	O17–Mo4–O8	92.8(4)	Mo5–O4–Mo2	115.3(4)
O11–Mo2–O9	97.0(5)	O17–Mo4–O18	104.5(5)	Mo5–O4–Mo4	102.9(4)
O16–Mo2–O4	98.7(4)	O17–Mo4–O19	102.9(5)	Mo1–O5–Ru1	143.6(5)
Ge1–O6–Mo2	118.9(4)	O18–Mo4–O4	92.3(4)	Ge1–O6–Mo1	120.3(4)
Ge1–O6–Mo5	122.9(4)	O18–Mo4–O7	156.3(4)	Mo5–O8–Mo4	103.6(4)
Mo1–O6–Mo2	95.5(3)	O18–Mo4–O8	90.0(4)	Mo2–O9–Mo2	142.9(7)
Mo1–O6–Mo5	95.9(3)	Mo1–O7–Mo4	102.6(4)	Mo2–O11–Mo3	145.3(5)
Mo5–O6–Mo2	97.3(3)	Mo2–O7–Mo1	112.5(5)	O5–Ru1–O2	86.3(3)
O2–Ru1–O2	178.7(5)	O5–Ru1–O1	91.5(3)	O5–Ru1–O2	92.7(3)
Ge1–O13–Mo3	125.5(4)	Mo1–O8–Mo4	104.9(4)	O5–Ru1–O2	86.3(3)
Mo3–O13–Mo3	95.5(5)	Mo1–O8–Mo5	112.1(4)	O5–Ru1–O2	92.7(3)
Mo3–O14–Mo3	116.7(6)	O1–Ru1–O1	85.0(5)	O5–Ru1–O5	92.3(5)
Mo3–O20–Na3	157.4(7)	O2–Ru1–O1	89.6(4)	O5–Ru1–O1	174.6(4)

Table S3 Calculated values of bond valence of Mo, Ge, Ru and O atoms in anion **$Ru_2Ge_2Mo_{20}$**.

Atom Lable	BVS	Atom Lable	BVS
Mo1	5.93	O8	1.886
Mo2	6.142	O9	2.099
Mo3	6.044	O10	1.707
Mo4	6.046	O11	1.894
Mo5	5.968	O12	2.049
Ru1	3.067	O13	1.822
Ge1	3.875	O14	1.894
O1	1.881	O15	1.666
O2	1.780	O16	1.846
O3	1.854	O17	1.583
O4	1.737	O18	1.578
O5	1.952	O19	1.570
O6	2.053	O20	1.635
O7	1.863		

Table S4 Comparison of similar photocatalytic CO_2 reduction systems based on POMs and some other materials.

Catalysts	Reactants	Light source	Photosensitizer sacrificial reagent	Major products (μmol g^{-1} h^{-1})	Ref.
$Na_{12}Rb_2[Ru_2O_2(GeMo_{10}O_{36})_2]\cdot 44H_2O$	CO_2, DMF, H_2O	300W Xe lamp (λ≥420nm)	$[Ru(bpy)_3]Cl_2\cdot 6H_2O$ TEOA	CH_4 91.31 CO 11.85	This work
NENU-605	CO_2, H_2O	300W Xe lamp (λ≥420nm)	$[Ru(bpy)_3]Cl_2\cdot 6H_2O$ TEOA	CH_4 0.894 CO 0.267	**3**
NENU-606				CH_4 1.747 CO 0.295	
$V_{12}B_{18}$–Co	CO_2, MeCN, H_2O	300W Xe lamp (λ≥420nm)	$[Ru(bpy)_3]Cl_2\cdot 6H_2O$ TEOA	CO 5700 H_2 3800 HCOOH 168	**4**
$V_{12}B_{18}$–Ni				CO 3200 H_2 300 HCOOH 260	
$[Co_{2.67}(SiW_{12}O_{40})(H_2O)_4(Htrz)_4]\cdot Cl_{1.33}$	CO_2, MeCN, H_2O	300W Xe lamp (λ≥420nm)	$[Ru(bpy)_3]Cl_2\cdot 6H_2O$ TEOA	CO 5235 H_2 4840	**5**
$[Co_3(SiW_{12}O_{40}(H_2O)_3(Htrz)_6Cl]\cdot Cl\cdot 6H_2O$				CO 6167 H_2 6070	
$(C_2H_5OH)(C_3H_5N_2)_6[Co_3(H_6P_4Mo_6O_{31})_2]\cdot H_2O$	CO_2, MeCN	300W Xe lamp (λ≥420nm)	$[Ru(bpy)_3]Cl_2\cdot 6H_2O$ TEOA	CO 723.6	**6**
$Na_6[Co(H_2O)_2(H_2tib)]_2\{Co[Mo_6{}^{V}O_{15}(HPO_4)_4]_2\}\cdot 5H_2O$	CO_2, H_2O	300W Xe lamp (λ≥420nm)	$[Ru(bpy)_3]Cl_2\cdot 6H_2O$ TEOA	CO 1.09 CH_4 0.042	**7**
$Na_3[Co(H_2O)_3][Co_2(bib)](H_2bib)_{2.5}\{HCo[Mo_6O_{14}(OH)(HPO_4)_4]_2\}\cdot 4H_2O$				CO 0.937 CH_4 0.035	
$(H_2bpp)_{1.5}\{Na[Mo_6O_{12}(OH)_3(HPO_4)(H_2PO_4)_3]_2\}\cdot 3H_2O$				CO 0.025 CH_4 0.005	
$[Ni_6(trz)_2(Htrz)_{13}][H_4P_4Mo_{11}O_{50}]\cdot 7H_2O$	CO_2, MeCN, H_2O	300W Xe lamp (λ≥420nm)	$[Ru(bpy)_3]Cl_2\cdot 6H_2O$ TEOA	CO 689.86 H_2 158.39	**8**
$[Co(H_2O)_6][Co\text{-}POM]$	CO_2, MeCN, H_2O	300W Xe lamp (λ≥420nm)	$[Ru(bpy)_3]Cl_2\cdot 6H_2O$ TEOA	syngas 33700	**9**
$K_{10}[Zn_4(H_2O)_2(PW_9O_{34})_2]\cdot 24H_2O$	CO_2, $KHCO_3$ solution	300W Xe lamp (λ≥400nm)	TIr_3 Na_2SO_3	CH_4 0.693	**10**
$H_7Na_{19}(H_2O)_{26}\{Ni_{12}(OH)_9(PO_4)_4(A\text{-}\alpha\text{-}SiW_9O_{34})[W_4O_{10}(OH)(PO_2(OH)_2)_2(A\text{-}\alpha\text{-}SiW_9O_{34})_2]\}\cdot 4C_2H_8N\cdot 27H_2O$ $H_{26.5}K_{2.5}Na(H_2O)_{16}[Ni_6(OH)(BO_3)_2(dien)_2(B\text{-}\alpha\text{-}SiW_{10}O_{37})_2]_2\cdot 24H_2O$	CO_2, MeCN, H_2O	300W Xe lamp (λ≥420nm)	$[Ru(bpy)_3]Cl_2\cdot 6H_2O$ TEOA	CO 1950 (1h) H_2 410 (1h) CO 6988 (1h) H_2 1315 (1h)	**11**
(Ru(bpy)-Mn)	CO_2, H_2O	280W Xe lamp (λ≥415nm)	$[Ru(bpy)_3]Cl_2\cdot 6H_2O$ TEOA	CH_4 0.6 CO 0.104	**12**
(Fe-Mn)				CH_4 1.44 CO 0.115	
$Co_2[Co_{20}Mo_{16}P_{24}]$	CO_2, MeCN, H_2O	300W Xe lamp (λ≥420nm)	$[Ru(bpy)_3]Cl_2\cdot 6H_2O$ TEOA	syngas 137900	**13**
$[Co@\{Co_{16}Mo_{16}\}]$	CO_2, MeCN	300W Xe lamp (λ≥420nm)	$[Ru(bpy)_3]Cl_2\cdot 6H_2O$ TEOA	CO 6764.3 (2h) 4489.3 (8h)	**14**
$[K(H_2O)_2Fe^{II}_{0.33}Co_{0.67}(H_2O)_2(DAPSC)]_2\{[Fe^{II}_{0.33}Co_{0.67}(H_2O)(DAPSC)]_2[Fe^{II}_{0.33}Co_{0.67}(H_2O)_4]_2[Na_2Fe^{III}_4P_4W_{32}O_{120}]\}\cdot 21.5H_2O$	CO_2, MeCN	300W Xe lamp (420-800nm)	$[Ru(bpy)_3]Cl_2\cdot 6H_2O$ TEOA	CH_4 135 H_2 568.3 CO 6881.5	**15**
$[Co(H_2O)_2DABT]_2[CrMo_6(OH)_5O_{19}]$	CO_2, MeCN	300W Xe lamp (420-800nm)	$[Ru(bpy)_3]Cl_2\cdot 6H_2O$ TEOA	CH_4 44.75 H_2 110.75 CO 1935.34	**16**
$[Zn(H_2O)_2DABT]_2[CrMo_6(OH)_5O_{19}]$				CO 82.018	
$H_{47}Na_2Co_4Mo_{24}(PO_4)_{11}O_{72}\cdot 15H_2O$	CO_2, MeCN	300W Xe lamp (420-800nm)	$[Ru(bpy)_3]Cl_2\cdot 6H_2O$ TEOA	CH_4 56.5 CO 1848.3	**17**
Ni MOLs	CO_2, MeCN, H_2O	5 W white LED light (420-800nm)	$[Ru(bpy)_3]Cl_2\cdot 6H_2O$ TEOA	syngas 12.78 mmol $g^{-1}h^{-1}$	**18**
ZIF-76				syngas 9 mmol g^{-1} h^{-1}	
Ni TDA MOFs				syngas 6.38 mmol $g^{-1}h^{-1}$	
Co TDA MOFs				syngas 4.92 mmol $g^{-1}h^{-1}$	
Ni MOLs				syngas 4.59 mmol $g^{-1}h^{-1}$	

Table S5 The apparent quantum yield of CH_4 and CO at different wavelength over **$Ru_2Ge_2Mo_{20}$**.

λ (nm)	CH_4 (μmol)	CO (μmol)	I ($W \cdot m^{-2}$)	AQY_{CH4} (%)	AQY_{CO} (%)
420	0.0628	0.0902	72.70	0.0093	0.0034
460	0.2385	0.1725	76.25	0.0308	0.0056
500	0.0431	0.1035	54.70	0.0071	0.0043
550	0.0410	0.0739	78.20	0.0042	0.0020

References

1. J. Xie, Y. Zhang, Y. Han and C. Li, High-Capacity Molecular Scale Conversion Anode Enabled by Hybridizing Cluster-Type Framework of High Loading with Amino-Functionalized Graphene, *ACS Nano*, 2016, **10**, 5304−5313.
2. J. G. Choi and L. T. Thompson, XPS study of as-prepared and reduced molybdenum oxides, *Appl. Surf. Sci.*, 1996, **93**, 143−149.
3. S.-L. Xie, J. Liu, L.-Z. Dong, S.-L. Li, Y.-Q. Lan and Z.-M. Su, Hetero-metallic active sites coupled with strongly reductive polyoxometalate for selective photocatalytic CO_2-to-CH_4 conversion in water, *Chem. Sci.*, 2019, **10**, 185−190.
4. X. Yu, C.-C. Zhao, J.-X. Gu, C.-Y. Sun, H.-Y. Zheng, L.-K. Yan, M. Sun, X.-L. Wang and Z.-M. Su, Transition-Metal-Modified Vanadoborate Clusters as Stable and Efficient Photocatalysts for CO_2 Reduction, *Inorg. Chem.*, 2021, **60**, 7364−7371.
5. W. Yao, C. Qin, N. Xu, J. Zhou, C. Sun, L. Liu and Z. Su, Visible-light CO_2 photoreduction of polyoxometalate-based hybrids with different cobalt clusters, *CrystEngComm*, 2019, **21**, 6423−6431.
6. Z.-Y. Du, Z. Chen, R.-K. Kang, Y.-M. Han, J. Ding, J.-P. Cao, W. Jiang, M. Fang, H. Mei and Y. Xu, Two 2D Layered P_4Mo_6 Clusters with Potential Bifunctional Properties: Proton Conduction and CO_2 Photoreduction, *Inorg. Chem.*, 2020, **59**, 12876−12883.
7. J. Du, Y. Ma, X. Xin, H. Na, Y. Zhao, H. Tan, Z. Han, Y. Li and Z. Kang, Reduced polyoxometalates and bipyridine ruthenium complex forming a tunable photocatalytic system for high efficient CO_2 reduction, *Chem. Eng. J.*, 2020, **398**, 125518.
8. M. Li, Y. Fu, S. You, Y. Yang, C. Qin, L. Zhao and Z. Su, Hexanuclear nickel-based $[P_4Mo_{11}O_{50}]$ with photocatalytic reduction of CO_2 activity, *Inorg. Chem. Commun.*, 2021, **134**, 109009.
9. X. Zhao, J. Zhou, C.-Y. Sun, S.-Q. You, X.-L. Wang and Z.-M. Su, A ruthenium/polyoxometalate for efficient CO_2 photoreduction under visible light in diluted CO_2, *Nanotechnology*, 2020, **31**, 255402.
10. N. Kim, J. S. Nam, J. Jo, J. Seong, H. Kim, Y. Kwon, M. S. Lah, J. H. Lee, T.-H. Kwon and J. Ryu, Selective photocatalytic production of CH_4 using Zn-based polyoxometalate as a nonconventional CO_2 reduction catalyst, *Nanoscale Horiz.*, 2021, **6**, 379−385.
11. Y. Chen, Z.-W. Guo, Y.-P. Chen, Z.-Y. Zhuang, G.-Q. Wang, X.-X. Li, S.-T. Zheng and G.-Y. Yang, Two novel nickel cluster substituted polyoxometalates: syntheses, structures and their photocatalytic activities, magnetic behaviors, and proton conduction properties, *Inorg. Chem. Front.*, 2021, **8**, 1303−1311.
12. Y. Benseghir, A. Solé-Daura, P. Mialane, J. Marrot, L. Dalecky, S. Béchu, M. Frégnaux, M. Gomez-Mingot, M. Fontecave, C. Mellot-Draznieks and A. Dolbecq, Understanding the Photocatalytic Reduction of CO_2 with Heterometallic Molybdenum(V) Phosphate Polyoxometalates in Aqueous Media, *ACS Catal.*, 2021, **12**, 453−464.

13. H. Xu, S. You, Z. Lang, Y. Sun, C. Sun, J. Zhou, X. Wang, Z. Kang and Z. Su, Highly Efficient Photoreduction of Low-Concentration CO_2 to Syngas by Using a Polyoxometalates/Ru^{II} Composite, *Chem. – Eur. J.*, 2020, **26**, 2735−2740.
14. C. Li, H.-Y. Jiang, J.-L. Wang, R.-K. Kang, H. Mei and Y. Xu, An isolated doughnut-like molybdenum(V) cobalto-phosphate cluster exhibiting excellent photocatalytic performance for carbon dioxide conversion, *Dalton Trans.*, 2022, **51**, 9616−9621.
15. J.-L. Zhou, X.-Y. Xiang, L.-T. Xu, J.-L. Wang, S.-M. Li, Y.-T. Yu, H. Mei and Y. Xu, Two bimetal-doped (Fe/Co, Mn) polyoxometalate-based hybrid compounds for visible-light-driven CO_2 reduction, *Dalton Trans.*, 2023, **52**, 9465−9471.
16. J.-B. Yang, J.-H. Pan, Y.-H. Zhu, J.-L. Wang, H. Mei and Y. Xu, Two 1D Anderson-Type Polyoxometalate-Based Metal–Organic Complexes as Bifunctional Heterogeneous Catalysts for CO_2 Photoreduction and Sulfur Oxidation, *Inorg. Chem.*, 2022, **61**, 11775−11786.
17. X. M. Liu, R. K. Kang, J. L. Wang, J. N. Li, Q. L. Chen and Y. Xu, A Purely Inorganic Quasi-Keggin Polyoxometalate for Photocatalytic Conversion of Carbon Dioxide to Carbon Monoxide, *ChemPlusChem*, 2021, **86**, 1014−1020.
18. B. Han, X. Ou, Z. Deng, Y. Song, C. Tian, H. Deng, Y. J. Xu and Z. Lin, Nickel Metal–Organic Framework Monolayers for Photoreduction of Diluted CO_2: Metal-Node-Dependent Activity and Selectivity, *Angew. Chem. Int. Ed.*, 2018, **57**, 16811−16815.